

POTASSIUM-INTERCALATED MANGANESE DIOXIDE AS LITHIUM-ION BATTERY CATHODES: A DENSITY FUNCTIONAL THEORY STUDY

Agus Ismail¹, Herry Agung Prabowo¹, Muhammad Hilmy Alfaruqi²

¹Department of Industrial Engineering, Universitas Mercu Buana
Jl. Raya Meruya Selatan, Kembangan, Jakarta 11650

²Department of Metallurgical Engineering, Universitas Teknologi Sumbawa
Jl. Raya Olat Maras, Sumbawa, Nusa Tenggara Barat 84371

Email: agus.ismail@mercubuana.ac.id, herry_agung@mercubuana.ac.id, hilmy@uts.ac.id

Abstract – It is obvious to harness the intermittent renewable energy resources, energy storage applications, such as a lithium-ion battery, are very important. α -type MnO_2 is considered as an attractive cathode material for lithium-ion battery due to its relatively large (2×2) tunnel structure, remarkable discharge capacity, low cost, and environmental benignity. However, low intrinsic electronic conductivity of α -type MnO_2 limits its full utilization as a cathode for a lithium-ion battery. Therefore, studies to enhance the α -type MnO_2 properties are undoubtedly of great interest. While previous computational studies have been focused on pristine α -type MnO_2 , in the present report, we present the theoretical research on potassium-intercalated α -type MnO_2 using first principle Density Functional Theory calculations for the first time. Our results showed that potassium-intercalated α -type MnO_2 improved the electronic conductivity which beneficial for energy storage application. The structural transformation of potassium-intercalated α -type MnO_2 upon lithium insertion are also discussed. Our results may open the avenue for further utilization of potassium-intercalated α -type MnO_2 materials for not only the lithium-ion battery but also other type energy storage systems.

Keywords: Manganese dioxide; Lithium-ion battery; Density functional theory

Received: December 31, 2018

Revised: January 28, 2018

Accepted: February 11, 2018

INTRODUCTION

Owing to the high population growth, indeed the demand for energy becomes unavoidable. Fossil-based energy, as one of the primary energy resources, is declining because oil reserves are dwindling (Nayak et al., 2018). Moreover, depending on the fossil-based energy is detrimental to our environment. Therefore, alternative energy resources, known as renewable energy such as solar, wind, tidal and geothermal energies have been intensively studied.

Nevertheless, these renewable energies are intermittent, and consequently, these systems should also have the ability to store the generated energy (Supegina & Imam, 2014). In this situation, rechargeable batteries as energy storage will be very urgent. Lithium-ion batteries (LIBs) are becoming a primary choice to fulfill that demand because of their high energies and power densities (Drewett et al., 2017; Nayak et al., 2018).

Besides, various technology advancement products such as digital cameras, drones, smartphones, laptops and some cases of tiny computers (Raspberry Pi) require batteries to power them (Divya & Ostergaard,

2009; Adriansyah et al., 2014; Supegina & Iklimia, 2015).

Transition metal oxides (TMOs) are one of the most attractive active materials for LIBs, particularly manganese oxides. In comparison with other TMOs such as Co and Ni-based oxides, Mn-based oxides are commonly used as cathode materials due to their low cost, low toxicity, and remarkable electrochemical performance (Li et al., 2018). Manganese dioxides (MnO_2) is amongst Mn-based oxides that have received great attention from the battery community. For example, Kim and co-workers reported the use of MnO_2 nanoflakes prepared via a reduction technique in basic medium (Kim et al., 2018). The cathode showed discharge and charge capacities of 477 and 223 mAh g^{-1} could be obtained at a current rate of 20 mA g^{-1} in the initial cycle. Moreover, the cathode exhibited 93% capacity retention after 200 cycles.

MnO_2 is known to exist in various crystallographic forms, for instance, α -, β -, γ -, δ -, λ -, and ϵ -type depending on how the fundamental unit of MnO_6 octahedral are connected, for example *via* edge- and/or corner-shared (Julien & Mauger, 2017). The α -

β - and γ -type exhibit 1-dimensional tunnels in their structures with (2×2) , (1×1) , and a combination of (1×1) and (2×1) tunnels, respectively. The δ -type has a 2-dimensional layered structure, while the λ -type shows a 3-dimensional spinel structure. Because of its (2×2) tunnel structure, α -type has obtained much interest in LIB applications experimentally as well as computationally. The large (2×2) tunnels facilitate the facile hosting/release of the charge carrier ions.

Density Functional Theory (DFT) is considered as an essential tool to study electrode materials properties for a battery application. DFT can be used to predict the structure, energetics, and electrochemical properties of electrode materials. As for α -type MnO_2 as LIB cathode, several reports studied its structure and Li-intercalation behavior. However, to the best of our knowledge, those reports have been focused on the primary and Li_2O -intercalated α -type MnO_2 , while it is widely known that initial α -type MnO_2 possesses low intrinsic electronic conductivity and leads to poor electrochemical properties (Ling & Mizuno, 2012; Tompsett & Islam, 2013). Therefore, in this contribution, we aim to fill the gap by performing DFT calculation to study the K-intercalated α -type MnO_2 structure and its Li-insertion properties for the first time. Our present study may provide an additional understanding to use K-intercalated α -type MnO_2 for a battery application. The potassium was selected in this study due to the potassium-containing precursors such as KMnO_4 is commonly used to synthesize α -type MnO_2 . Literature also records that particular alkali-ion also plays a significant role in forming α -type MnO_2 with a tetragonal system (Kitchaev et al., 2018).

METHOD

In this work, we performed density functional theory (DFT) calculations as implemented in the Quantum-Espresso package using projector augmented wave (PAW) pseudopotential and Perdew-Burke-Emzerhof (PBE) exchange-correlation functional (Giannozzi et al., 2009).

A plane-wave basis set with a cutoff of 25 Ry (340 eV) was used for all calculations. The atoms in the α -type MnO_2 structure (space group $I4/m$) were relaxed using Broyden-Fletcher-Goldfarb-Shanno (BFGS) scheme with energy and force convergences criteria of 1×10^{-4} Ry and 1×10^{-3} Ry/Bohr, respectively, wherein all the axes and angles were permitted to move freely.

The Brillouin zone was sampled using a k-point mesh of $3 \times 3 \times 3$ and $1 \times 1 \times 2$ supercells was used. All crystallographic figures were drawn using VESTA software (Momma, Izumi, 2011).

RESULTS AND DISCUSSION

LIB commonly consists of anode, cathode, and electrolyte. The anode is generally made from carbon (graphite) for full cell configuration or Li metal anode for half-cell system while the cathode is typically formed from a transition metal compound such as oxide or phosphate-based compound. In principle, LIBs work in mostly the same way.

Individually, when the battery is discharging, the lithium ions move across the electrolyte to the cathode, generating the energy that can power up the electronic devices, and reversely, when the battery is charging up, the cathode releases its Li-ions, which move to the anode through the electrolyte. The LIB mechanism is illustrated in Fig. 1. Amongst transition metal oxide compounds, MnO_2 , particularly α -type MnO_2 has obtained a significant interest.

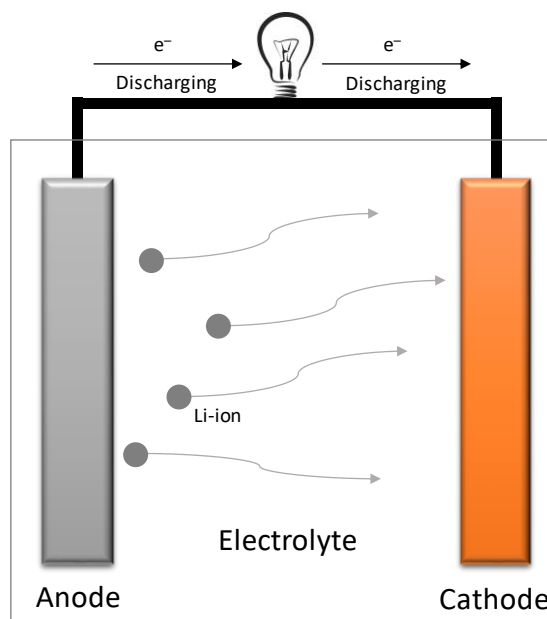


Figure 1. Illustration of LIB components and its corresponding mechanism.

α -type MnO_2 has a relatively large (2×2) tunnels along the c -axis within the structure. α -type MnO_2 also exhibits tetragonal symmetry which belongs to $I4/m$ space group (No. 87). α -type MnO_2 built of edge-shared MnO_6 octahedral units, and its structure is shown in Fig. 2, while the formation of K-intercalated α -type MnO_2 is depicted in Fig. 3. In the present study, the

intercalated K is located in the center of the (2×2) tunnels of α -type MnO_2 structure ($2a$ sites). Literature recorded that metal-intercalated α -type MnO_2 enhanced the electrical conductivity, for example, Co- or V-intercalated α -type MnO_2 . Due to the relatively high cost and toxicity of cobalt and vanadium, thus potassium is used. Potassium is considered low cost, abundance and environmentally benign.

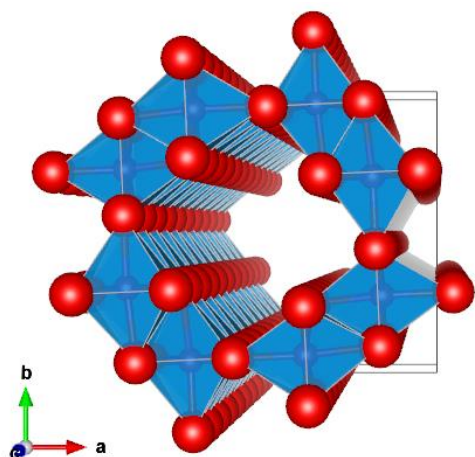


Figure 2. Illustration of α -type MnO_2 crystallographic structure. Red color is oxygen while blue is MnO_6 octahedral unit.

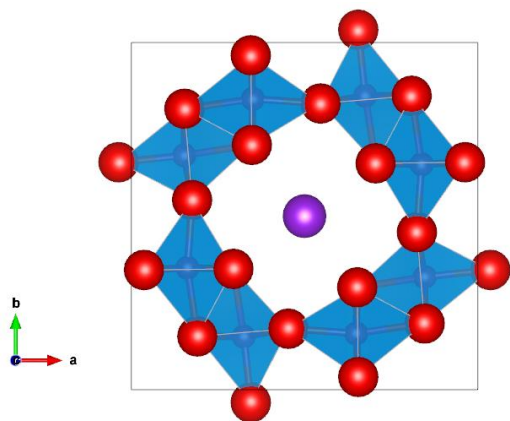


Figure 3. Illustration of K-intercalated α -type MnO_2 crystallographic structure. A big purple sphere is K.

The calculated unit cell parameters of the relaxed pristine α -type MnO_2 structure were $a = b = 9.45$ and $c = 2.79$ Å, and the values are in agreement with the experimental results previously reported (Johnson, et al., 1997). After K-intercalation, the unit cell parameters were calculated to be $a = b = 9.53$ and $c = 2.79$ Å. Also, the unit cell volumes of the relaxed pristine

and K-intercalated α -type MnO_2 were 250.32 and 253.91 Å³, respectively; thus, the K-intercalation into α -type MnO_2 only expands the unit cell slightly, i.e., approximately 1.4%, without collapsing the structure. The expansion also advantages for further Li-ion insertion/extraction into/from the structure.

To study the improved electrical conductivity of K-intercalated α -type MnO_2 , a density of state (DOS) calculations were performed. The total DOS for pristine and K-intercalated α -type MnO_2 are shown in Fig. 4. It can be seen that the initial α -type MnO_2 showed semiconducting behavior with a distinct bandgap, while the K-intercalated α -type MnO_2 showed occupied spin-down states inside the pristine α -type MnO_2 bandgap, indicating the enhanced conductivity of α -type MnO_2 after K-ion intercalation.

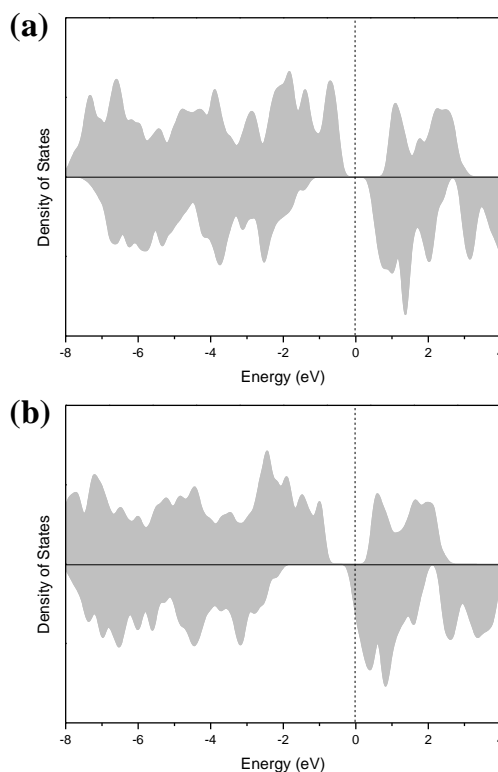


Figure 4. Electron density of states of (a) primary α -type MnO_2 and (b) K-intercalated α -type MnO_2 calculated using DFT.

For use as cathode materials for LIBs, studies of the insertion of Li-ion into α -type MnO_2 suggested that the tunnels might facilitate the insertion. In the present case, since K-ions is located at $2a$ sites, we consider at least two possible sites for Li-ions to reside, namely $2b$ and $8h$ sites, depicted in Fig. 5a. $2b$ sites are positioned at the center of the (2×2) tunnels

adjacent to $2a$ sites, whereas $8h$ sites are situated close to $2a$ and $2b$ sites with a small deviation, toward the pseudocubic walls (Fig. 5b).

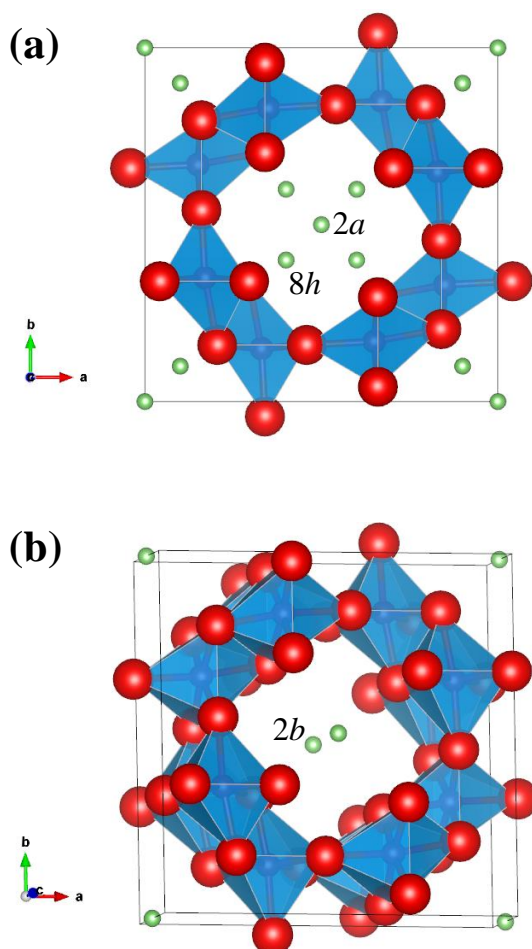


Figure 5. Possible insertion sites in α -type MnO_2 structure. (a) $8h$ and (b) $2b$ sites.

Cause of considering the above-mentioned available sites in the (2×2) tunnels, the Li-ions were further the added and structural relaxations were also performed. In the beginning, we calculated the dilute limit of Li-insertion. Specifically, only one Li-ion was put in a $1 \times 1 \times 2$ supercell of α -type MnO_2 structure (16 Mn and 31 O atoms). In the dilute limit, the compound composition is expressed as α -type $\text{Li}_1\text{K}_2\text{Mn}_{16}\text{O}_{32}$ or α -type $\text{Li}_{0.0625}\text{K}_{0.125}\text{MnO}_2$. The insertion energy was calculated as a function of concentration using Equ. (1).

$$E_l = E_{\text{Li}_1\text{K}_2\text{Mn}_{16}\text{O}_{32}} - E_{\text{K}_2\text{Mn}_{16}\text{O}_{32}} - E_{\text{Li}} \quad (1)$$

where $E_{\text{Li}_1\text{K}_2\text{Mn}_{16}\text{O}_{32}}$ is the energy of $\text{Li}_1\text{K}_2\text{Mn}_{16}\text{O}_{32}$, $E_{\text{K}_2\text{Mn}_{16}\text{O}_{32}}$ is the energy of $\text{K}_2\text{Mn}_{16}\text{O}_{32}$ and E_{Li} is the energy of Li.

Our calculation suggested that the site preference for Li-ion in the dilute limit is $8h$ site due to an $8h$ site having lower insertion energy compared to that of a $2b$ site within 40 meV. Our calculation is in agreement with the previous report (Tompsett & Islam, 2013). We note that the structural model used in the Tompsett and Islam's calculation was pristine α -type MnO_2 , whereas, in our report, we employed K-intercalated α -type MnO_2 . However, a similar tendency was also found in our present results. We note also that the Li-ion insertion in the dilute limit increases the unit volume ca. 0.87%. It is also worth mentioning here that the insertion of Li-ion in the dilute limit results in a slight change of the joint angle between MnO_6 octahedral units from 82.12 to 83.15° .

We then proceeded our calculations for Li-ion insertion into α -type MnO_2 structure beyond the dilute limit and the calculated lattice parameters and unit cell volumes are presented in Table 1. For the concentration of $\text{Li}_{0.125}\text{K}_{0.125}\text{MnO}_2$, $\text{Li}_{0.25}\text{K}_{0.125}\text{MnO}_2$ and $\text{Li}_{0.5}\text{K}_{0.125}\text{MnO}_2$, the calculated unit cell volumes were 258.25, 262.57 and 278.21 \AA^3 , respectively. Interestingly, the calculated a/b ratio for the $\text{Li}_{0.5}\text{K}_{0.125}\text{MnO}_2$ is 1. The a/b ratio is commonly used to indicate Jahn-Teller distortion phenomena when it shows a value larger than 1 within the concentration $\text{Li}_{0.5}\text{MnO}_2$. Here, the K-intercalation is shown to effectively stabilize the structure. This will be beneficial for long term cycling of the electrode.

Table 1. Calculated lattice parameters and unit cell volumes for lithium-inserted $\text{K}_{0.125}\text{MnO}_2$

Composition	a (Å)	b (Å)	c (Å)	V (Å ³)
$\text{Li}_{0.125}\text{K}_{0.125}\text{MnO}_2$	9.51	9.72	2.79	258.25
$\text{Li}_{0.25}\text{K}_{0.125}\text{MnO}_2$	9.69	9.69	2.79	262.57
$\text{Li}_{0.5}\text{K}_{0.125}\text{MnO}_2$	9.87	9.87	2.85	278.21
$\text{Li}_{1.0}\text{K}_{0.125}\text{MnO}_2$	10.12	10.12	2.82	289.43

Fig. 6 illustrates the structure of α -type $\text{Li}_{0.5}\text{K}_{0.125}\text{MnO}_2$. The structure remains tetragonal symmetry after the insertion of 0.5 moles of lithium. It was previously reported the insertion of other cation such as Mg (0.5 moles) cause severe deformation of α -type MnO_2 structure. Ling et al. highlighted that the α -type MnO_2 structure was barely maintained (Ling & Mizuno, 2012).

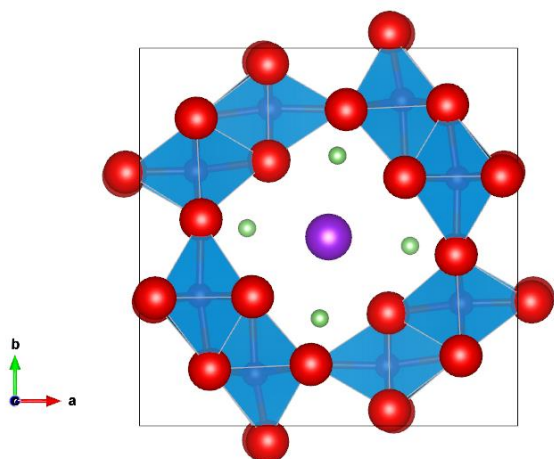


Figure 6. Relaxed α -type $\text{Li}_{0.5}\text{K}_{0.125}\text{MnO}_2$ structure.

Furthermore, from Fig. 7 it is obvious that the unit cell of α -type MnO_2 structure expanded largely causing the stretch of the octahedral MnO_6 . The final a and c lattice parameters were 10.12 and 2.82 Å, while the unit cell volume 289.43 Å³. However, the unit cell volume change was only about 13.8%, which is lower than that of pristine α -type MnO_2 after 1-mole Li-ion intercalation (Tompsett & Islam, 2013). Therefore, the strategy of using K-intercalation in α -type MnO_2 structure may be useful for further development of monovalent as well as multivalent battery systems.

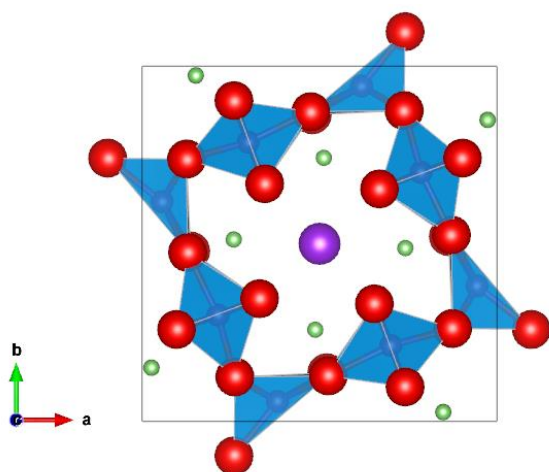


Figure 7. Relaxed α -type $\text{K}_{0.125}\text{MnO}_2$ structure after 1-mole Li-ion insertion showing the stretch of MnO_6 octahedral unit.

CONCLUSION

In conclusion, we have performed first-principles calculations to assess the insertion

behavior of Li-ion in K-intercalated α -type MnO_2 structure for Li-ion battery-based energy storage. Our estimates suggest the preferred Li-insertion site in K-intercalated α -type MnO_2 structure is an $8h$ site. We also show that K-intercalation into α -type MnO_2 strategy may increase the electronic conductivity and further prevent large unit cell volume expansion upon Li-ion insertion, by only 13.8% after 1 mole of Li-ion insertion, which is lower than that of pristine α -type MnO_2 . Finally, this study provides theoretical information for further use and development α -type MnO_2 structure in energy storage system towards its practical application and commercialization.

REFERENCES

- Adriansyah, A., Rizki, G.M.M. & Yuliza. (2014). Rancangbangun dan analisa CCTV online berbasis Raspberry Pi. *SINERGI*, 18(2), 105-110.
- Divya, K.C. & Ostergaard, J. (2009). Battery energy storage technology for power systems – An overview. *Electric Power Systems Research*. 79(4), 511-520. <http://doi.org/10.1016/j.epsr.2008.09.017>
- Drewett, N.E., Aldous, I.M., Zou, J.L. & Hardwick, L.J. (2017). In situ Raman spectroscopic analysis of the lithiation and sodiation of antimony microparticles. *Electrochim Acta*, 247(1), 296–305. <http://doi.org/10.1016/j.electacta.2017.07.030>
- Giannozzi et al. (2015). Quantum ESPRESSO: a modular and open-source software project for quantum simulations of materials. *Journal of Physics: Condensed Matter*, 21(39), 395502-395521. <https://doi.org/10.1088/0953-8984/21/39/395502>
- Julien, C.M. & Mauger, A. (2017). Nanostructured MnO_2 as electrode materials for energy storage. *Nanomaterials*, 7(11), 1-42. <http://doi.org/10.3390/nano7110396>
- Kitchaev, D.A., Dacek, S.T., Sun, W., & Ceder, G. (2017). Thermodynamics of phase selection in MnO_2 framework structures through alkali intercalation and hydration, *Journal of the American Chemical Society*, 139(7), 2672-2681. <http://dx.doi.org/10.1021/jacs.6b11301>
- Kim, K., Daniel, G., Kessler, V.G., Seisenbaeva, G.A., Pol, V.G. (2018). Basic medium heterogeneous solution synthesis of α - MnO_2 nanoflakes as an anode or cathode in half cell configuration (vs. lithium) of Li-ion batteries *Nanomaterials*, 8(8), 1-12. <https://dx.doi.org/10.3390/nano8080608>

- Li, M., Lu, J., Chen, Z. & Amine, K. (2018). 30 years of lithium-ion batteries. *Advanced Materials*, 30(33), 1-24/
<http://doi.org/10.1002/adma.201800561>
- Ling, C. & Mizuno, F. (2012). Capture lithium in αMnO_2 : insights from first principles. *Chemistry of Materials*, 24(20), 3943-3951.
<http://dx.doi.org/10.1021/cm302347j>
- Momma, K. & Izumi F. (2011). VESTA 3 for three-dimensional visualization of crystal, volumetric and morphology data. *Journal of Applied Crystallography*, 44(6), 1272-1276.
<https://dx.doi.org/10.1107/S0021889811038970>
- Nayak, P.K. et al. (2018). Review on challenges and recent advances in the electrochemical performance of high capacity Li- and Mn-rich cathode materials for Li-ion batteries, *Advanced Energy Materials*, 8, 1702397.
<http://doi.org/10.1002/aenm.201702397>
- Supegina, F. & Iklima, Z. (2015). Perancangan scoreboard dan timer menggunakan LED RGB berbasis arduino dengan kendali smart phone android. *SINERGI*, 19(1), 13-18.
<http://dx.doi.org/10.22441/sinergi.2015.1.003>
- Supegina, F. & Imam. (2014). Pengaturan lampu taman LED RGB berbasis Arduino yang dilengkapi solar cell. *SINERGI*, 18(1), 9-14.
- Tompsett, D.A. & Islam, M.S. (2013). Electrochemistry of hollandite $\alpha\text{-MnO}_2$: Li-ion and Na-ion insertion and Li_2O incorporation. *Chemistry of Materials*, 25(12), 2515-2526.
<http://dx.doi.org/10.1021/cm400864n>